iScience

CellPress
OPEN ACCESS

Article

The non-adrenergic imidazoline-1 receptor protein nischarin is a key regulator of astrocyte glutamate uptake

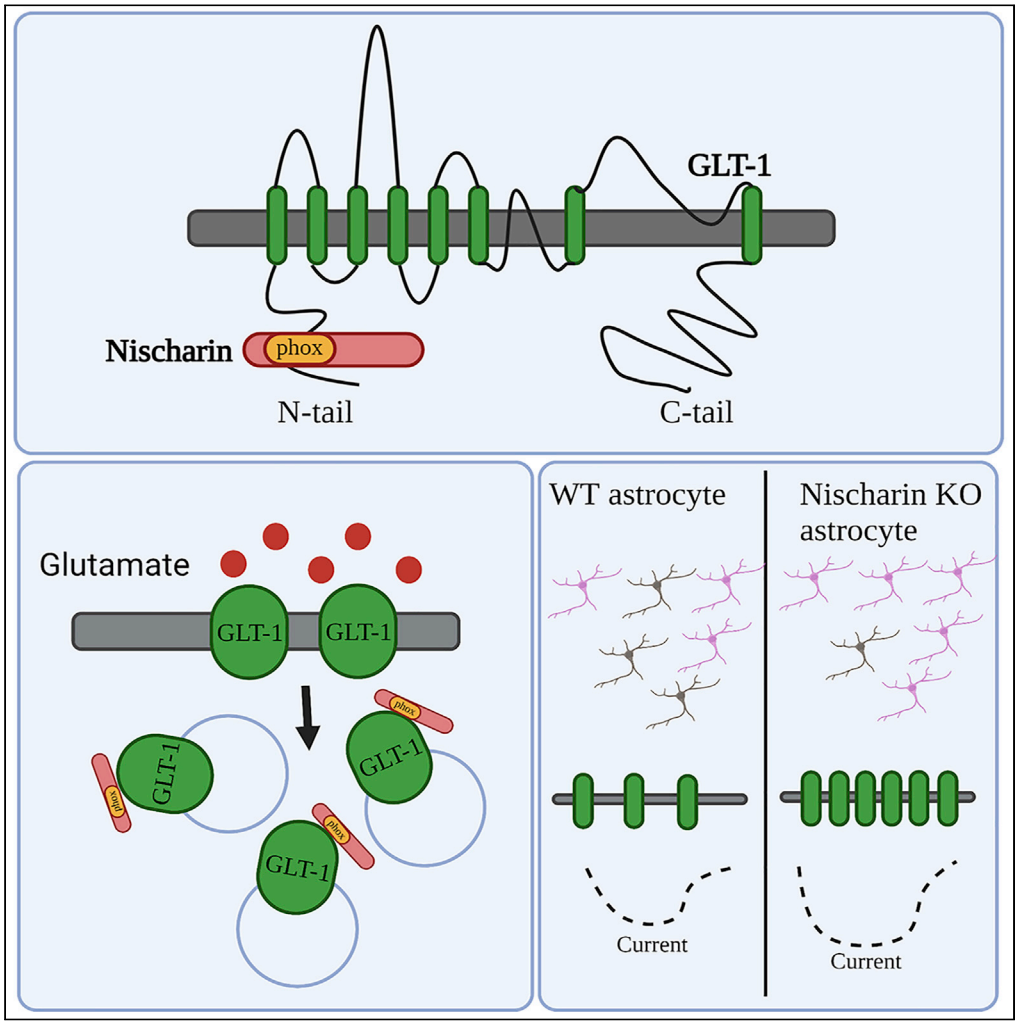

Swati Gupta, Narges Bazargani, James Drew, ..., Hélène Marie, David Attwell, Josef T. Kittler

j.kittler@ucl.ac.uk

Highlights

Nischarin phox domain interacts with the N-terminus of the glutamate transporter, GLT-1

Nischarin promotes internalization of GLT-1 to endosomes

Glutamate modulates GLT-1 surface levels by regulating the Nischarin-GLT-1 interaction

Nischarin loss enhances GLT-1 surface levels, transport currents, and neuroprotection

Gupta et al., iScience *25*, 104127
April 15, 2022
https://doi.org/10.1016/j.isci.2022.104127

iScience

CellPress
OPEN ACCESS

Article

The non-adrenergic imidazoline-1 receptor protein nischarin is a key regulator of astrocyte glutamate uptake

Swati Gupta,[1,2] Narges Bazargani,[1] James Drew,[1,3] Jack H. Howden,[1] Souvik Modi,[1,6] Sana Al Awabdh,[1,4] Hélène Marie,[1,5] David Attwell,[1] and Josef T. Kittler[1,7,*]

SUMMARY

Astrocytic GLT-1 is the main glutamate transporter involved in glutamate buffering in the brain, pivotal for glutamate removal at excitatory synapses to terminate neurotransmission and for preventing excitotoxicity. We show here that the surface expression and function of GLT-1 can be rapidly modulated through the interaction of its N-terminus with the nonadrenergic imidazoline-1 receptor protein, Nischarin. The phox domain of Nischarin is critical for interaction and internalization of surface GLT-1. Using live super-resolution imaging, we found that glutamate accelerated Nischarin-GLT-1 internalization into endosomal structures. The surface GLT-1 level increased in Nischarin knockout astrocytes, and this correlated with a significant increase in transporter uptake current. In addition, Nischarin knockout in astrocytes is neuroprotective against glutamate excitotoxicity. These data provide new molecular insights into regulation of GLT-1 surface level and function and suggest new drug targets for the treatment of neurological disorders.

INTRODUCTION

Glutamate transport into cells is mediated by excitatory amino acid transporters (EAATs). Of the five EAAT subtypes found in the CNS, EAAT2/GLT-1 is predominantly expressed in astrocytes and is a major means for glutamate clearance from the extracellular space (Danbolt, 2001). Glutamate buffering through transporter binding helps to maintain a low extracellular glutamate concentration that facilitates termination of fast excitatory synaptic transmission (Diamond and Jahr, 1997; Wadiche et al., 1995a, 1995b; Tong and Jahr, 1994). Moreover, lateral diffusion of surface GLT-1 can also regulate glutamate clearance and thus shape glutamatergic neurotransmission (Al Awabdh et al., 2016; Murphy-Royal et al., 2015). The transporters have a long transport cycle (~70 ms) (Wadiche et al., 1995a) compared to the timescale of glutamate presence at the synapse (~1 ms) (Barbour and Hausser, 1997). However, despite this long transport cycle, efficient glutamate clearance occurs during synaptic activity because of the high surface density of transporters (Danbolt, 2001). A low extracellular glutamate concentration (below the submicromolar level that tonically activates NMDA receptors) is also crucial to prevent excitotoxic cell death (Choi et al., 1987; Choi, 1987). Thus, control of GLT-1 density on the astrocyte surface via molecular mechanisms modulating its intracellular trafficking is crucial for normal synaptic physiology and prevention of excitotoxicity.

Four isoforms of GLT-1 have been identified, which exhibit similar functional properties and oligomerize to form homomeric and heteromeric GLT-1 pools. However, the GLT-1 isoforms differ in their N- and C-termini, allowing for interaction with different intracellular proteins and offering an opportunity for differential regulation of the isoforms during physiological and pathological conditions (Peacey et al., 2009). So far, scaffolding proteins, such as PSD-95, PICK-1, and MAGI-1 have been shown to interact with the PDZ domain containing C-terminus of the GLT-1b isoform (Underhill et al., 2015; Sogaard et al., 2013; Zou et al., 2011; Gonzalez-Gonzalez et al., 2008). Here, we have identified the non-adrenergic imidazoline-1 receptor protein Nischarin, as a new physiological GLT-1 N-terminus interacting protein in astrocytes. Nischarin is a cytoplasmic protein that shows a diverse set of functions, including regulation of the cytoskeletal network (through Rac1), interaction with endosomes (via its phox domain), and regulation of receptor (mu opioid and integrin α_5 receptors) surface levels (Alahari et al., 2000, 2004; Keller et al., 2017; Li et al., 2016; Kuijl et al., 2013; Alahari, 2003; Dong et al., 2017).

[1]Department of Neuroscience, Physiology and Pharmacology, University College London, Gower Street, WC1E 6BT London, UK

[2]Present address: Nash Family Department of Neuroscience and Friedman Brain Institute, The Icahn School of Medicine at Mount Sinai, New York 10029, NY, UK

[3]Present address: Beatson Institute for Cancer Research, Garscube Estate, Switchback Road, Bearsden, Glasgow G61 1BD, UK

[4]Present address: INSERM UMR-S 1123, Université de Paris, 75006 Paris, France

[5]Present address: Université Côte d'Azur, CNRS UMR 7275, IPMC, Valbonne, France

[6]Present address: Esya Ltd. Imperial College White City Campus, Translation and Innovation Hub, 84 Wood Lane, W12 0BZ, UK

[7]Lead contact

*Correspondence: j.kittler@ucl.ac.uk

https://doi.org/10.1016/j.isci.2022.104127

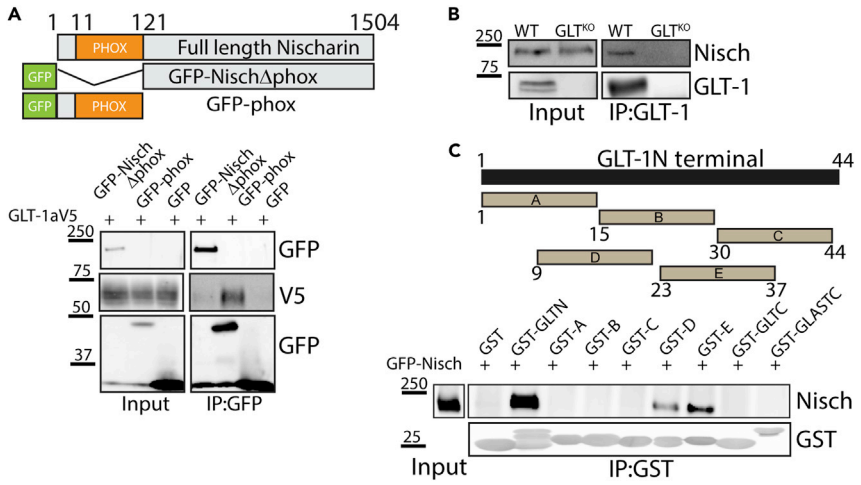

Figure 1. The phox domain of Nischarin interacts with GLT-1

(A) Schematic diagram depicting full length Nischarin and GFP-tagged mutants. GLT-1aV5 coimmunoprecipitated with GFP-phox but not GFP-NischΔphox mutant or GFP control.

(B) Coimmunoprecipitation experiments from mouse brain homogenate from WT and GLT^{KO} mice, showing Nischarin to be part of a native complex with GLT-1 (n = 3).

(C) Schematic diagram of GST fusion constructs for GLT-1 N-terminus, 15 amino acid stretches of GLT-1 N-terminus (A-E), GLT-1 C-terminus, and GLAST C-terminus. GFP-Nisch was successfully pulled down with full-length GST-fused GLT-1 N-terminus and to GST fusions D (amino acids 9-23) and E (amino acids 23-37).

Here, we report that the Nischarin phox domain is sufficient for interaction with a 30 amino acid stretch of the GLT-1 N-terminus. Super-resolution imaging revealed that glutamate drives internalization of GLT-1 in a Nischarin-dependent pathway. In addition, Nischarin knockout (Nisch^{KO}) animals exhibit increased astrocytic GLT-1 surface expression that correlates with increased transporter current and enhanced neuroprotection. Together, these data suggest a new molecular mechanism by which glutamatergic signaling is regulated in the CNS under both physiological and pathological conditions.

RESULTS

GLT-1 and Nischarin interact *in vivo*

A yeast two-hybrid screen (Y2H) with the GLT-1 N-terminus identified a clone that encoded the phox domain of the Nischarin protein as a molecular interactor for the GLT-1 protein (Marie et al., 2002). Next, a coimmunoprecipitation assay was performed in COS cells co-transfected with GLT-1a (tagged in the extracellular loop with a V5 epitope) and GFP-tagged Nischarin (Nisch) lacking the phox domain (GFP-NischΔphox), or Nischarin's phox domain alone (GFP-phox) or a GFP control (Figure 1A). We found that the GFP-phox domain construct, but not the GFP-NischΔphox, coprecipitated with GLT-1 (Figure 1A), suggesting that the phox domain of Nischarin is sufficient for the interaction with GLT-1. In parallel experiments, coimmunoprecipitation assays in brain lysates generated from adult wild-type (WT) and GLT-1 knockout (GLT^{KO}) animals confirmed the interaction between Nischarin and GLT-1 protein in WT mice, which was lacking in the GLT^{KO} mice (Figure 1B). Western blotting in cortical astrocytes derived from rat pups (P0-P2) confirmed expression of endogenous Nischarin (Figure S1A).

Using a GST fusion assay, we further narrowed down the binding region within the N-terminal tail of GLT-1 participating in the interaction with Nischarin. The following GST-tagged fusion proteins were used as bait; 1) full-length GLT-1 N-terminus fusion protein, 2) fusion proteins containing overlapping stretches (15 amino acid in length) of the GLT-1 N-terminus (A-E), 3) full-length GLT-C-terminus, and 4) full-length GLAST C-terminus, to assess pull down of Nischarin from lysates of GFP-Nisch or GFP transfected COS cells. Although the N-terminus of GLT-1 successfully interacted with Nischarin, its C-terminal end and that of GLAST did not. Interestingly, within the GLT N-terminal, two 15 amino acid stretches from 9-24 and 23-37 successfully interacted with Nischarin (Figure 1C). Given that the other GST fused GLT-1 N terminal segments did not interact with Nischarin, this implies that the Nischarin binding site on GLT-1 is complex and that the two sites (9-24 and 23-27) are sufficient for binding Nischarin, independently.

Nischarin promotes endocytosis and not recycling of GLT-1

Nischarin has been shown to alter the surface levels of receptors, including integrins and mu opioid receptors (Li et al., 2016, 2019; Lim and Hong, 2004). To determine whether Nischarin regulated GLT-1 surface density, we used an 'antibody-feeding' immunofluorescence internalization assay in HeLa cells to visualize GLT-1 trafficking. HeLa cells were co-transfected with GLT-1 tagged in its extracellular domain with HA (GLT-1a-HA) along with either GFP-Nisch or GFP as a control. Briefly, antibody against the HA tag, present in the extracellular loop of GLT-1, was incubated with the cells for 15 min before placing them in the incubator at 37°C for 60 min to allow for internalization, followed by differential immunostaining of the surface and internal GLT-1 pool. To obtain a reference value for basal surface GLT-1 levels before internalization, cells were fixed immediately after the antibody surface labeling (constituting the T_{0min} population). At baseline (T_{0min}), in control cells, robust surface and low internal GLT-1 labeling was observed. Even after 60 min, a significant change in GLT-1 internalization was not observed in the control (Figures 2A and 2C), suggesting stable turnover of the transporter under basal culture conditions. In GFP-Nisch expressing cells, no significant difference was observed in GLT-1 distribution initially at T_{0min}; however, by 60 min, significant increases were observed in the accumulation of GLT-1 within intracellular compartments (Figures 2B and 2C). This suggests that Nischarin regulates constitutive trafficking of GLT-1 under basal conditions.

As trafficking of GLT-1 is dependent on endocytic and recycling pathways, we next assessed the effects of Nischarin on GLT-1 recycling. No significant differences were found between the GLT-1 recycling rates in GFP-Nisch cells and control (Figures S1B–S1D). Together, these data suggest that Nischarin promotes translocation of GLT-1 from the surface to intracellular compartments but (in contrast to its effect on mu opioid receptors: Li et al., 2016) does not affect GLT-1 recycling.

Next, astrocytes were transfected with either GFP-Nisch or GFP-NischΔphox or GFP control, and were cocultured with hippocampal neurons. At DIV 14, immunostaining studies revealed significant colocalization between GFP-Nisch-positive endosomal structures and the early endosomal marker EEA1. The GFP-Nisch-positive vesicles showed variability in size and shape and were distributed throughout the astrocyte cell body and processes. However, GFP-Δphox showed a cytosolic expression, corroborating previous reports that Nischarin is targeted to endosomes via its phox domain (Figures S1A–S1D). In addition, endogenous GLT-1 co-localized significantly with intracellular vesicles positive for GFP-Nisch (Figure 2E). Together these data suggest that intracellular GLT-1 accumulates in Nischarin-positive early endosomal structures within the astrocyte cell body and processes.

Glutamate promotes Nischarin-mediated GLT-1 intracellular trafficking in fixed and live hippocampal astrocyte cultures

It has been previously reported that glutamate treatment decreases clustering and surface expression of GLT-1 (Al Awabdh et al., 2016; Underhill et al., 2015). The PDZ-binding domain containing protein DLG1 interacts with the C-terminal PDZ ligand of GLT-1b to regulate its surface density (Underhill et al., 2015). However, the role of molecules interacting with the N terminus of GLT-1 remains under explored. Therefore, we investigated whether Nischarin regulates GLT-1 trafficking under activity driven conditions, which we mimicked by applying glutamate.

Using a surface biotinylation assay, the effect of glutamate on surface GLT-1 levels in Nischarin-overexpressing astrocytes was assessed. Pure cortical astrocyte cultures were co-transfected with GFP and GLT-1a tagged with V5 (control) or GFP-Nisch and GLT-1a-V5. The transfected cultures were either left untreated or exposed to glutamate (100 μM, 1 h). Glutamate treatment significantly decreased surface GLT-1 level compared to the untreated control (Figure 3A), as expected (Ibanez et al., 2016). Nischarin overexpression significantly decreased the GLT-1 surface levels compared to the untreated control in the absence of glutamate, corroborating our findings in Figure 2. Glutamate treatment in Nischarin-overexpressing astrocytes did not cause any further decrease in surface GLT-1 levels in comparison to Nischarin overexpression or glutamate application alone, suggesting that overexpression of Nischarin alone is sufficient to drive the internalization of surface GLT-1.

Next, using a proximity ligation assay (PLA), a powerful tool that detects a positive protein interaction only if the two proteins are closer than 40 nm, we determined the effect of glutamate on the endogenous GLT-1-Nischarin interaction. In DIV14 hippocampal cultures, under control conditions, a significant increase in

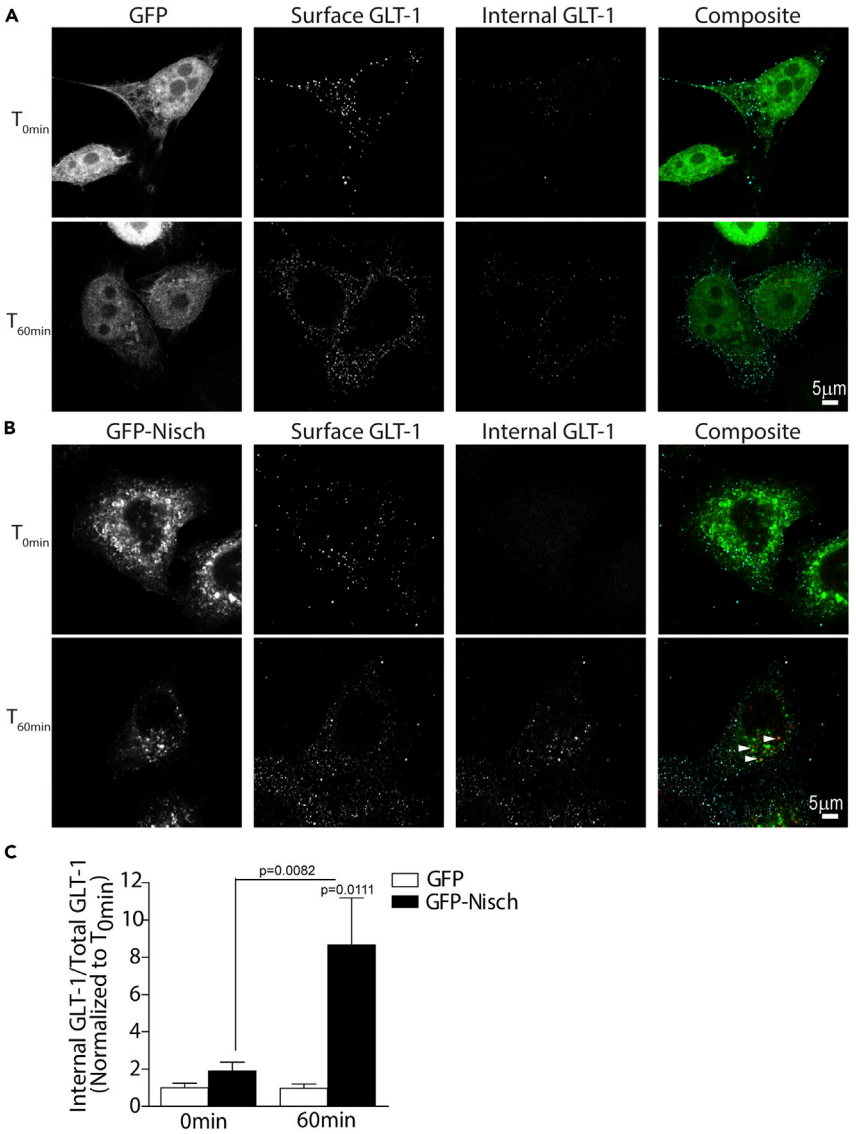

Figure 2. Antibody feeding assay revealed that Nischarin promotes internalization of GLT-1

(A–C). Surface and internal GLT-1 populations labeled in HeLa cells co-expressing (A) GFP and GLT-1a-HA or (B) GFP-Nisch and GLT-1a-HA at 0 min and 60 min. (C) Quantification of internalized GLT-1 to total GLT-1 levels at $T_{60\ min}$ relative to $T_{0\ min}$. One-way ANOVA, Kruskal-Wallis test with Dunn's correction (n = 12).

Nischarin-GLT-1 direct association (assessed by number of red puncta per DAPI-labeled (blue) nuclei) was observed compared to single antibody (Nisch/GLT-1) controls. Upon glutamate treatment (100 μM, 1 h), the number of puncta observed were significantly increased compared to the control (Figure 3B). Together with the biotinylation assay, these results suggest that glutamate enhances the endogenous GLT-1-Nischarin interaction, and that this drives internalization of surface GLT-1.

To monitor live trafficking of GLT-1, we took advantage of a high affinity 13 amino acid α-bungarotoxin (BTX)-binding site (BBS) that has been exploited for tracking AMPA receptor movements in and out of the cell membrane (Sekine-Aizawa and Huganir, 2004). We explored a similar strategy to assess the time course of glutamate's action on the GLT-1-Nischarin interaction by engineering the extracellular loop of the GLT-1 transporter (Figure 3C) to include the BBS tag. This position in GLT-1 transporters is silent in terms of its impact on receptor structure and function (Peacey et al., 2009). The astrocytes were co-transfected with GLT-1a-BBS and GFP-Nisch and cocultured with hippocampal neurons. The hippocampal

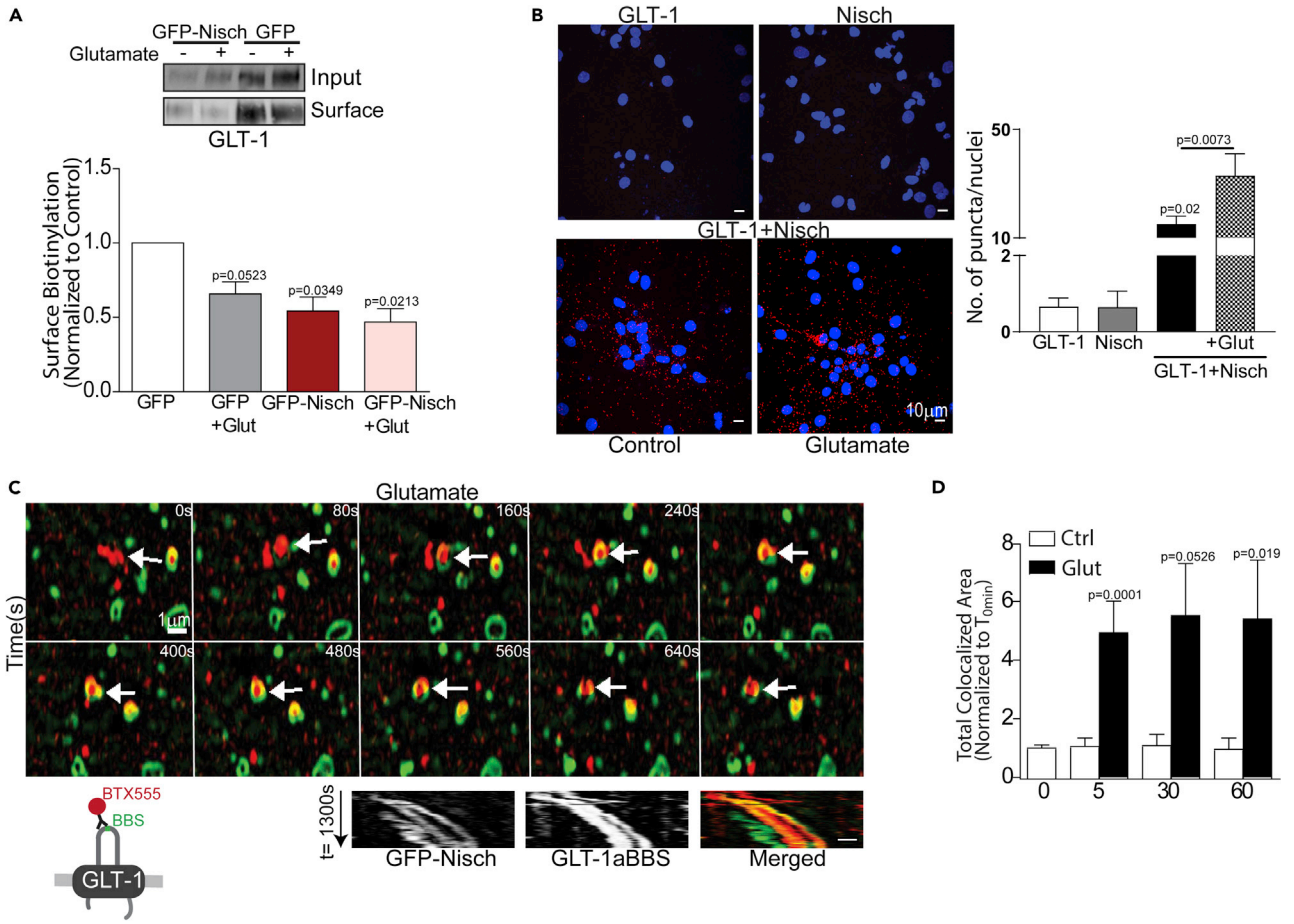

Figure 3. Nischarin mediates glutamate-dependent GLT-1 internalization in astrocytes

(A) Surface biotinylation assay showing surface GLT-1 level in astrocytes transfected with GFP and GLT-1a-V5 or GFP-Nisch and GLT-1a-V5 following +/− 100µM glutamate treatment. One-way ANOVA, post hoc Dunnett's multiple comparison test (n = 4 individual experiments).

(B) Proximity ligation assay in DIV14 hippocampal culture. Increased red puncta per nuclei (DAPI stained (blue)) is indicative of increased direct interaction between Nischarin and GLT-1 in hippocampal culture. Glutamate treatment (100µM, 1h) significantly increased GLT-1-Nischarin interaction compared to control. One-way ANOVA, post hoc Tukey's test (n = 3 individual preparations).

(C) Schematic representation of GLT-1BBS construct bound to BTX conjugated Alexa 555 (BTX555). Astrocytes expressing GFP-Nisch and GLT-1aBBS were labeled using BTX555 and dual color live-structured illumination microscopy-monitored trafficking of GLT-1 following glutamate treatment. Merged kymographs of GFP-Nisch vesicle (green) and GLT-1 bound BTX-555 (red) reveal co-localized diagonal trajectory, representing moving vesicles.

(D) Quantification of GFP-Nisch and GLT-1aBBS expressing astrocytes treated with 100µM glutamate for 0, 5, 30, and 60min showed increased colocalization between Nisch and GLT-1 compared to untreated controls. p values by unpaired *t* test, Mann Whitney test (n = 6-14).

coculture was incubated with Alexa 555-conjugated BTX (BTX555) at 37°C for 20 min to allow live labeling of surface GLT-1. Live time-lapse imaging using structured-illumination microscopy (SIM)-tracked transporter internalization and individual endosomal events in labeled GLT-1a-BBS astrocytes (cocultured with hippocampal neurons) co-expressing GFP-Nisch and exposed to ACSF alone or ACSF containing 100µM glutamate (Figure 3C). GFP-Nisch-positive intracellular vesicles were observed within the astrocyte processes and cell body. Glutamate application resulted in internalization of BTX555-labeled surface GLT-1 transporters to GFP-Nisch-labeled vesicles, as seen by the diagonal and co-localized lines in the kymographs representing GLT-1 and Nischarin vesicle movements within the astrocyte process (Figure 3C). GFP-Nisch was found to be associated with the inner plasma membrane, and the internalized surface GLT-1 was trafficked into GFP-Nisch-positive vesicles, pinched off from the plasma membrane (Videos S1 and S2).

Using the same setup as described above, the cocultures were exposed to varying durations (5, 30, or 60 min) of glutamate (100 or 0 µM) and subsequently fixed and imaged using confocal microscopy to ascertain the time course of Nischarin-mediated GLT-1 trafficking. GLT-1 showed increased colocalization with

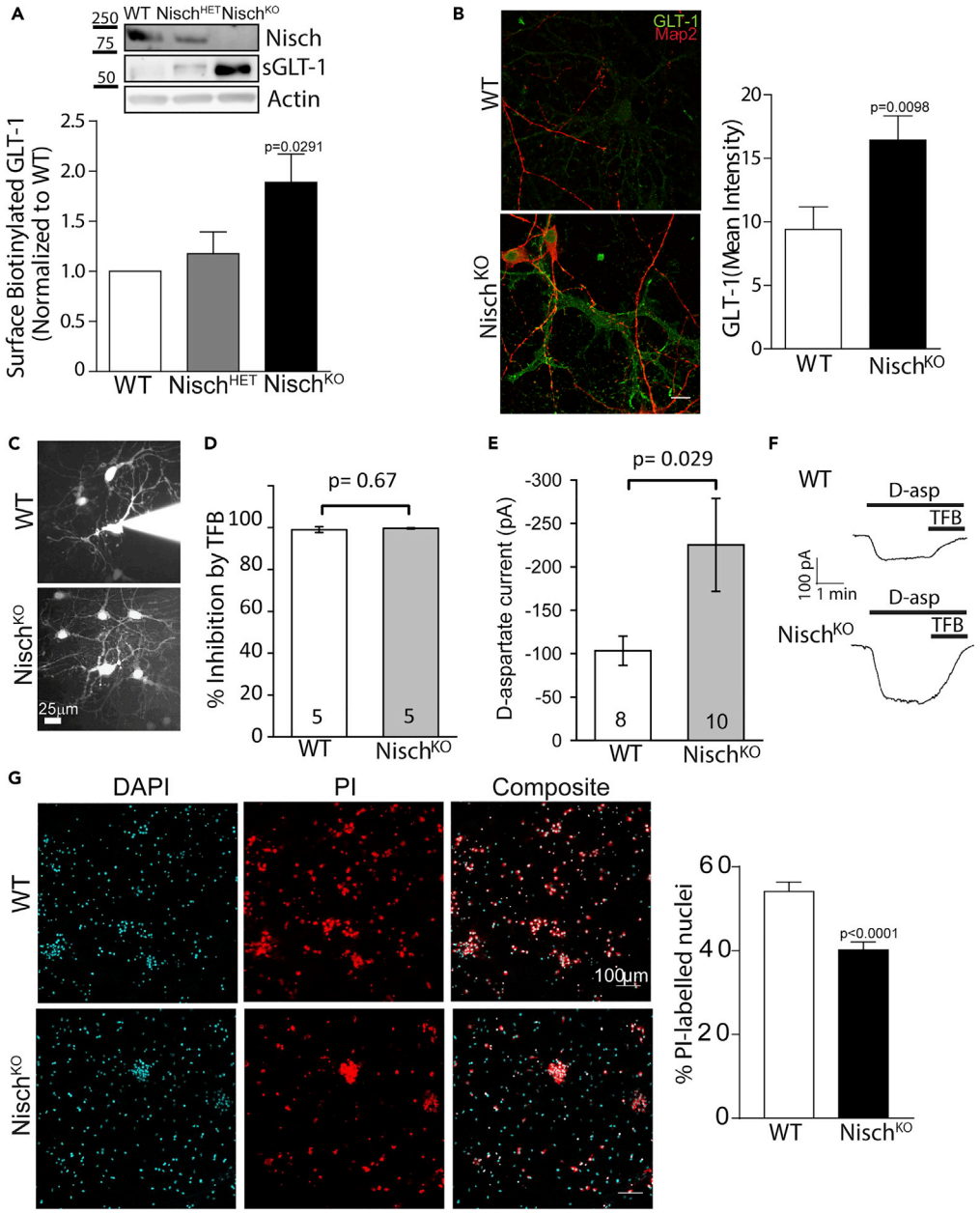

Figure 4. GLT-1 surface density and transporter uptake current are enhanced in Nisch^{KO} astrocytes

(A) Western blot analysis in cortical astrocytes derived from WT, Nisch^{HET}, and Nisch^{KO} E16 embryos, confirmed decrease and loss of Nischarin in the HET and KO cultures. Surface biotinylation assay showed significant increase in GLT-1 surface density in KO culture compared to WT control. One-way ANOVA, post hoc Tukey's test (n = 3 animals).

(B) Representative images for GLT-1 (green) and Map2 (red) immunostaining in astrocytes derived from DIV14 WT and Nisch^{KO} hippocampal culture. A significant increase in GLT-1 mean fluorescence intensity was observed in Nisch^{KO} astrocytes. Unpaired Student's *t* test (n = 11-13).

(C) Examples of astrocytes filled with Alexa 488 from the patch pipette (still attached to the cell for the WT and after electrode removal for the Nisch^{KO}) in WT and Nisch^{KO} hippocampal tissue cultures.

(D) The D-aspartate evoked current is completely blocked by TFB-TBOA.

(E) A significantly larger D-aspartate evoked current was recorded in the Nisch^{KO} astrocytes compared to the WT, unpaired student t-tests.

(F) Sample traces showing the D-aspartate evoked (200 µM) current and its inhibition by the GLT-1 and GLAST transporter blocker TFB-TBOA (TFB, 10 µM), in WT and Nisch^{KO} astrocytes.

Figure 4. *Continued*
(G) Representative confocal images showing nuclear staining DAPI (cyan) and PI labeling (red) in DIV 14 WT and Nisch^{KO} hippocampal culture, 24h following a glutamate insult. Bar graph showing percentage of PI-labeled nuclei (n = 3, unpaired two-tailed t-test).

GFP-Nisch-labeled vesicles (in white, Figure S3A) upon glutamate treatment in comparison to control at all three time points (Figure 3D). Together, these results reinforce the role of Nischarin in regulating GLT-1 internalization during glutamate application, with colocalization observed as early as 5 min. Further investigation in to the subcellular localization of the co-localized GFP-Nisch vesicles containing BTX-labeled GLT-1 transporters revealed even distribution across the astrocyte cell body and processes in control and glutamate-treated (100mM, 60 min) cultures (Figures S4A–S4D).

GLT-1 transporter density and function are altered in Nisch^{KO} mice

We further characterized the role of Nischarin-mediated regulation of astrocytic GLT-1 by using transgenic Nisch^{KO} mice (Figures S3B–S3D). Lack of Nischarin expression was confirmed in homozygous Nisch^{KO} mice, whereas the heterozygous (Nisch^{HET}) mice showed reduced Nischarin protein expression in comparison to the WT control (Figure 4A). A surface biotinylation assay revealed significant increases in surface GLT-1 levels in astrocytes derived from Nisch^{KO} transgenic mice compared to from WT control mice. The surface GLT-1 level in astrocytes derived from Nisch^{HET} transgenics were not significantly different from that of WT (Figure 4A). Immunostaining studies also revealed a significant increase in total astrocytic GLT-1 mean intensity in hippocampal cocultures derived from Nisch^{KO} mice in comparison to WT control (Figure 4B), which may reflect trafficking to a degradation pathway in the absence of Nischarin. These data support Nischarin's role in regulating GLT-1 surface levels.

Given the increased surface GLT-1 level in Nisch^{KO} astrocytes, we undertook functional studies where glutamate uptake was assessed using whole cell patch-clamp of astrocytes in hippocampal neuron-glial cocultures (Brew and Attwell, 1987). For each glutamate anion transported into astrocytes by GLT-1, three Na^+ and one H^+ are also transported in, and one K^+ is exported from the cell (Levy et al., 1998a, 1998b; Zerangue and Kavanaugh, 1996). Thus, two net positive charges are imported per glutamate taken up; therefore, uptake can be measured from the current it produces. Astrocytes were whole cell patch clamped and their identity was confirmed by the following: 1) dye filling (Alexa 488 or 594) to show coupling with other astrocytes (Figure 4C), 2) their low input resistance (Figures S5A and S3), and 3) their negative resting potential (Figure S5B). The input resistance and resting potential were not significantly affected by knockout of Nischarin (Figures S5A and S5B). After applying blockers of action potentials (150 nM TTX), inward-rectifying K^+ channels i.e., the main conductance of astrocytes (200 μM $BaCl_2$), and glutamate and GABA receptors (blocked with 10 μM NBQX, 50 μM D-AP5, 10 μM 5,7-dichlorokynurenate, 10 μM MK-801, and 10 μM bicuculline), once a steady membrane current was reached, at a voltage near the cell's resting potential (−90 mV), glutamate transporters were activated by applying D-aspartate (200 μM). D-aspartate evoked an inward current in both WT and Nisch^{KO} astrocytes (Figure 4E). The currents were confirmed to be mediated by glutamate transporters, because they were blocked by the GLT-1 and GLAST blocker TFB-TBOA (10 μM Figures 4D and 4F). Consistent with the surface biotinylation assay, we found that the glutamate uptake current was almost 2-fold higher in the Nisch^{KO} astrocytes in comparison to the WT astrocytes ($p = 0.029$, Figures 4E and 4F).

Dysfunction of glutamate clearance can cause overstimulation of glutamate receptors and result in neuronal injury, termed excitotoxicity. To further investigate the neuroprotective function of astrocytes, we carried out an excitotoxicity assay using hippocampal neuron -astrocyte cocultures derived from WT and Nisch^{KO} mice (at DIV 14). The cultures were challenged with 10 μM glutamate and 10 μM glycine for 24 h. Neuronal death was analyzed using propidium iodide (PI) and DAPI staining, and the number of PI-positive nuclei (red) were counted. Glutamate treatment evoked significantly less PI-labeling of neurons in Nisch^{KO} cocultures compared with neurons in wild type cocultures (Figure 4G). These data suggest that when challenged with neurotoxic glutamate levels, lack of Nischarin is protective against cell death, presumably because of the increased glutamate uptake that lack of Nischarin results in.

DISCUSSION

Glutamatergic neurons are responsible for the majority of the excitatory synaptic transmission and plasticity occurring in the brain. The astrocytic glutamate transporters serve the critical role of efficiently

clearing glutamate from the extracellular space (Tanaka et al., 1997) to ensure normal glutamate signaling. GLT-1 is one of the highest expressed proteins in the brain (1% of total brain protein (Lehre and Danbolt, 1998). The high number of surface glutamate transporters (GLT-1 at a density of 8,500 transporters/μm^2 as well as GLAST at 2,500 transporters/μm^2) compensate for the slow transport cycle (12-70ms) to ensure effective clearance of the ~4000 glutamate molecules released from a single synaptic vesicle (Lehre and Danbolt, 1998; Murphy-Royal et al., 2017). GLT-1 undergoes activity-dependent surface diffusion, and the glutamate-bound GLT-1 from 'synapse facing' sites are continuously replaced with GLT-1-lacking-bound glutamate to help maintain a high concentration of available surface transporters at the astrocytic plasma membrane (Murphy-Royal et al., 2017; Al Awabdh et al., 2016). Thus, an in-depth understanding of the molecular mechanisms regulating and maintaining the surface GLT-1 density is crucial. Here, we have identified a new interacting protein partner, Nischarin, a non-adrenergic imidazoline-1 receptor (Alahari, 2003) that regulates intracellular trafficking of GLT-1 in response to the neurotransmitter glutamate. Further work is needed to establish whether the blood pressure lowering effects of imidazoline drugs such as clonidine are in any way mediated by effects on glutamate transport.

We found that Nischarin interacts with the N-terminal tail of GLT-1 through its phox domain. Specifically, Nischarin coprecipitated with amino acids 9-37 within the intracellular, unstructured N-terminal tail of GLT-1. Amino acids 9-23 have also been implicated in the interaction with Ajuba, a scaffolding protein that allows GLT-1 to regulate intracellular signaling or interact with the cytoskeleton (Marie et al., 2002). These amino acids are conserved across the four GLT-1 isoforms (Peacey et al., 2009), suggesting Nischarin could regulate all four isoforms, unlike previously identified regulators of GLT-1 trafficking that bind specifically to the PDZ domain found in GLT-1b (Bassan et al., 2008; Underhill et al., 2015). In addition, a coimmunoprecipitation assay using brain lysates confirmed that the Nischarin-GLT-1 interaction occurs in the intact brain. As we have only examined immunoprecipitation assays from the whole brain, we considered whether regional variation in the Nisch-GLT-1 interaction might occur. However, Nischarin protein levels detected using the same antibody as our study are comparable in the cortex and hippocampus (Ding et al., 2013); therefore, differences in GLT-1 binding capacity are unlikely. Glutamate transporters are known to interact with Na,K-ATPases and can exist with them as part of one macromolecular complex (Rose et al., 2009). Whether Nischarin is able to regulate the entire Glt-1/Na,K-ATPase macromolecular complex remains to be determined. The findings reported here do raise the intriguing possibility that, in addition to Nischarin's previously reported role in regulating cytoskeletal signaling, cell migration, Rab-dependent endosomal sorting, and regulation of integrins and mu opioid receptors (Keller et al., 2017; Kuijl et al., 2013; Alahari, 2003), it may have an activity-dependent role in modulating glutamate concentration at the synapse.

GLT-1 is known to undergo constitutive and regulated endocytosis, which determines its availability for glutamate clearance from extracellular compartments in the nervous system (Martinez-Villarreal et al., 2012). Our antibody-feeding assays have revealed that overexpression of Nischarin redistributed surface GLT-1 transporters into endosomal structures but did not alter transporter recycling under basal conditions. Taken together, our data not only support an interaction between Nischarin and GLT-1 but also indicate the possibility that Nischarin alters trafficking of GLT-1 by sequestration. The phox domain of Nischarin is a stretch of ~110 amino acids that is a phosphatidylinositol 3-phosphate-binding (PI3P) module, and PI3P is enriched in early endosomal membranes (Lim and Hong, 2004). Our data confirmed previous findings that Nischarin is targeted to early endosomes, marked by EEA1 (Kuijl et al., 2013), but also showed multiple Nischarin-positive yet EEA1-negative vesicular structures, revealing a much wider distribution of Nischarin within the endosomal system. In addition, we observed that the GLT-1-Nischarin vesicular structures are spatially distributed along the astrocyte cell body and processes.

Surface biotinylation studies revealed that astrocytic GLT-1 surface levels decreased (40%) in response to glutamate (Figure 3A), which is consistent with previous findings (Ibanez et al., 2016). Overexpressing Nischarin in astrocytes exposed to glutamate treatment did not significantly further alter surface GLT-1 levels, implying that Nischarin occludes the effect of glutamate on surface GLT-1. Alteration in surface GLT-1 levels by Nischarin could offer a means for modulating glutamatergic activity at the synapse. Given the increased Nisch-GLT-1 interaction following glutamate exposure, a likely explanation for these results is that Nischarin mediates the effects of glutamate-dependent GLT-1 surface density regulation. The recruitment of Nischarin to GLT-1 could have additional consequences as Nischarin is known to act as a scaffolding platform for signaling pathways through its interactions with multiple proteins including, integrin

α5, PAK, Rac, LIMK, and ERK (Alahari, 2003; Alahari et al., 2000; Juliano et al., 2004). The Nischarin-LIMK pathway is of particular interest as it directly impacts cofilin-1 phosphorylation (Ding et al., 2008), a key effector protein that regulates LTP induced withdrawal of perisynaptic astroglial processes (PAPs) (Henneberger et al., 2020). The removal of PAPs from the synapse can boost glutamate spillover and shape NMDA-receptor-mediated inter-synaptic cross-talk (Henneberger et al., 2020).

Using time-lapse monitoring of the transporter (employing a GLT-1aBBS construct that can bind fluorophore-conjugated BTX, eliminating the use of bulky antibodies which could promote clustering and affect membrane trafficking properties (Sekine-Aizawa and Huganir, 2004)), we showed that glutamate binding and/or transport triggered intracellular trafficking of GLT-1 into Nischarin-labeled intracellular compartments within 5 min of glutamate exposure and is evenly distributed across the astrocyte cell body and processes. This time course suggests that the GLT-1-Nisch trafficking could be of more relevance in pathological conditions such as ischemia or traumatic brain injury, where the extracellular concentration of glutamate remains elevated (in the 100-200 μM range) for hours (Ibanez et al., 2016). Future studies should focus on a wider range of glutamate concentrations, and examine the GLT-1-Nisch interaction in astrocytes following neuronal stimulation to ascertain its functional relevance during synaptic activity. SIM resolution allowed tracking of single GFP-Nisch-labeled vesicles containing GLT-1BBS bound BTX555, and the resultant kymograph confirmed colocalization and inwardly directed (toward the cell body), slow (∼minutes) movement as vesicles traversed the astrocytic process.

Astrocytes derived from Nisch^{KO} transgenic animals exhibit increased surface GLT-1 density and a concomitant 2-fold increase in transporter uptake currents. Future experiments should examine how Nisch KO affects the EPSCs generated by neuronal action potentials, especially during high frequency stimulation or activation of many axons when clearance of glutamate from the synaptic cleft becomes more critically dependent on glutamate transporter activity. This enhanced surface GLT-1 density served to reduce cell death after glutamate insult, demonstrating the relevance of this mechanism to pathology. Dysregulation of Nischarin regulation of GLT-1 transporter surface density and function could affect glutamate clearance. Ineffective glutamate clearance is observed in many neurodegenerative diseases, including amyotrophic lateral sclerosis, epilepsy, Alzheimer's, Huntington's, and Parkinson's disease (Hindeya Gebreyesus and Gebrehiwot Gebremichael, 2020; Peterson and Binder, 2019). Therefore, this work not only reveals a distinct mechanism by which GLT-1 intracellular trafficking and function are regulated but also provides possible new avenues of research for treating neurological disorders.

Limitations of the study

We found that the N-terminal domains of Glt-1 (residues 9-27) are sufficient for the interaction with Nischarin. Future studies should further identify the precise amino acid residues on Glt-1, which would help to allow selective targeting of this interaction to control glutamatergic transmission. In addition, previous studies found that Glt-1 regulation is mediated by phosphorylation. It would be interesting to determine the role of phosphorylation in regulating the Glt-1 – Nischarin interaction. As shown and discussed in the text, most of the imaging results of this study were derived from an *in vitro* primary astrocyte-neuron cell culture model systems. Further microscopy studies will be needed to validate the effect of Nischarin on Glt-1 membrane dynamics in more intact tissue. However, confirmation in more intact tissue systems (acute brain slices) of the impact on Glt-1 function was achieved using electrophysiology.

STAR★METHODS

Detailed methods are provided in the online version of this paper and include the following:

- KEY RESOURCES TABLE
- RESOURCE AVAILABILITY
  - Lead contact
  - Materials availability
  - Data and code availability
- EXPERIMENTAL MODEL AND SUBJECT DETAILS
  - Cell culture
  - Transgenic animal
- METHOD DETAILS
  - Yeast two-hybrid screen

- Plasmid constructs
- Preparation and transfection of astrocyte cultures
- Preparation and transfection of mixed culture and the neuron-astrocyte co-cultures
- Cell culture and transfection
- Coimmunoprecipitation assays from rat brain homogenate and cell culture
- Western blotting
- GST pull down assays from transfected COS7 cells
- Biotinylation assay
- Excitotoxicity assay
- Proximity ligation assay
- Antibody feeding
- Immunostaining
- Live imaging
- Electrophysiology
- Recording glutamate uptake in astrocytes

● QUANTIFICATION AND STATISTICAL ANALYSIS

SUPPLEMENTAL INFORMATION

Supplemental information can be found online at https://doi.org/10.1016/j.isci.2022.104127.

ACKNOWLEDGMENTS

This work was supported by grants from the BBSRC (BB/I00274X/1) and European Research Council grant 282430 (Fueling Synapses) to J.T.K. S.M. was supported by an EMBO Long-Term Fellowship and Marie Skłodowska-Curie International Incoming Fellowship (Nos. 630033 and 913033). This work was also supported by a PhD studentship from the Medical Research Council (MRC) to J.D. (1477260) and a Wellcome Trust 4-year PhD studentship in Neuroscience to N.B. D.A. was supported by an Investigator Awards (099222/Z/12/Z and 219366/Z/19/Z) from the Wellcome Trust. We thank all members of the Kittler laboratory for helpful discussions and comments. We also thank the Light Microscopy facility at the MRC Laboratory for Molecular Cell Biology SURF facility for training and technical support. Graphical abstract was created with Biorender.com.

AUTHOR CONTRIBUTIONS

Conceptualization, S.G. and J.T.K.; Methodology, S.G., N.B., J.D., S.M., and J,H.; Formal Analysis, S.G., N.B., J.D., S.M., and J.H.; Investigation, S.G., N.B., J.D., S.M., H.M., and J.H.; Writing – Original Draft, S.G.; Writing – Review & Editing, S.G., N.B., D.A., and J.T.K.; Visualization, S.G., N.B., J.D., and S.M., and J.H.; Supervision, D.A. and J.T.K.; Funding Acquisition, D.A. and J.T.K.

DECLARATION OF INTERESTS

The authors declare no competing interests.

Received: December 28, 2020
Revised: December 24, 2021
Accepted: March 17, 2022
Published: April 15, 2022

REFERENCES

Al Awabdh, S., Gupta-Agarwal, S., Sheehan, D.F., Muir, J., Norkett, R., Twelvetrees, A.E., Griffin, L.D., and Kittler, J.T. (2016). Neuronal activity mediated regulation of glutamate transporter glt-1 surface diffusion in rat astrocytes in dissociated and slice cultures. Glia *64*, 1252–1264.

Alahari, S.K. (2003). Nischarin inhibits rac induced migration and invasion of epithelial cells by affecting signaling cascades involving pak. Exp. Cell Res. *288*, 415–424.

Alahari, S.K., Lee, J.W., and Juliano, R.L. (2000). Nischarin, A novel protein that interacts with the integrin Alpha5 subunit and inhibits cell migration. J. Cell Biol. *151*, 1141–1154.

Alahari, S.K., Reddig, P.J., and Juliano, R.L. (2004). The integrin-binding protein nischarin regulates cell migration by inhibiting pak. Embo J. *23*, 2777–2788.

Arancibia-Carcamo, I.L., Yuen, E.Y., Muir, J., Lumb, M.J., Michels, G., Saliba, R.S., Smart, T.G., Yan, Z., Kittler, J.T., and Moss, S.J. (2009). Ubiquitin-dependent lysosomal targeting of gaba(A) receptors regulates neuronal inhibition. Proc. Natl. Acad. Sci. U S A. *106*, 17552–17557.

Banker, G., and Goslin, K. (1998). Culturing Nerve Cells (MIT Press).

Barbour, B., Brew, H., and Attwell, D. (1991). Electrogenic uptake of glutamate and aspartate into glial cells isolated from the salamander

(Ambystoma) retina. J. Physiol. *436*, 169–193. https://doi.org/10.1113/jphysiol.1991.sp018545.

Barbour, B., and Hausser, M. (1997). Intersynaptic diffusion of neurotransmitter. Trends Neurosci. *20*, 377–384.

Bassan, M., Liu, H., Madsen, K.L., Armsen, W., Zhou, J., Desilva, T., Chen, W., Paradise, A., Brasch, M.A., Staudinger, J., et al. (2008). Interaction between the glutamate transporter Glt1b and the synaptic pdz domain protein Pick1. Eur. J. Neurosci. *27*, 66–82.

Brew, H., and Attwell, D. (1987). Electrogenic glutamate uptake is A major current carrier in the membrane of axolotl retinal glial cells. Nature *327*, 707–709.

Choi, D.W. (1987). Ionic dependence of glutamate neurotoxicity. J. Neurosci. *7*, 369–379.

Choi, D.W., Maulucci-Gedde, M., and Kriegstein, A.R. (1987). Glutamate neurotoxicity in cortical cell culture. J. Neurosci. *7*, 357–368.

Danbolt, N.C. (2001). Glutamate uptake. Prog. Neurobiol. *65*, 1–105.

Davies, L.P., and Johnston, G.A. (1976). Uptake and release of D- and L-aspartate by rat brain slices. J. Neurochem. *26*, 1007–1014. https://doi.org/10.1111/j.1471-4159.1976.tb06485.x.

Diamond, J.S., and Jahr, C.E. (1997). Transporters buffer synaptically released glutamate on A submillisecond time scale. J. Neurosci. *17*, 4672–4687.

Ding, Y., Milosavljevic, T., and Alahari, S.K. (2008). Nischarin inhibits Lim kinase to regulate cofilin phosphorylation and cell invasion. Mol. Cell Biol. *28*, 3742–3756.

Ding, Y., Zhang, R., Zhang, K., Lv, X., Chen, Y., Li, A., Wang, L., Zhang, X., and Xia, Q. (2013). Nischarin is differentially expressed in rat brain and regulates neuronal migration. Plos One *8*, E54563.

Dong, S., Baranwal, S., Garcia, A., Serrano-Gomez, S.J., Eastlack, S., Iwakuma, T., Mercante, D., Mauvais-Jarvis, F., and Alahari, S.K. (2017). Nischarin inhibition alters energy metabolism by activating amp-activated protein kinase. J. Biol. Chem. *292*, 16833–16846.

Furness, D.N., Dehnes, Y., Akhtar, A.Q., Rossi, D.J., Hamann, M., Grutle, N.J., Gundersen, V., Holmseth, S., Lehre, K.P., Ullensvang, K., et al. (2008). A quantitative assessment of glutamate uptake into hippocampal synaptic terminals and astrocytes: new insights into a neuronal role for excitatory amino acid transporter 2 (EAAT2). Neuroscience *157*, 80–94. https://doi.org/10.1016/j.neuroscience.2008.08.043.

Gong, X.Q., Frandsen, A., Lu, W.Y., Wan, Y., Zabek, R.L., Pickering, D.S., and Bai, D. (2005). D-aspartate and NMDA, but not L-aspartate, block AMPA receptors in rat hippocampal neurons. Br. J. Pharmacol. *145*, 449–459. https://doi.org/10.1038/sj.bjp.0706199.

Gonzalez-Gonzalez, I.M., Garcia-Tardon, N., Cubelos, B., Gimenez, C., and Zafra, F. (2008). The glutamate transporter Glt1b interacts with the scaffold protein psd-95. J. Neurochem. *105*, 1834–1848.

Henneberger, C., Bard, L., Panatier, A., Reynolds, J.P., Kopach, O., Medvedev, N.I., Minge, D., Herde, M.K., Anders, S., Kraev, I., et al. (2020). Ltp induction boosts glutamate spillover by driving withdrawal of perisynaptic astroglia. Neuron *108*, 919–936.e11.

Hindeya Gebreyesus, H., and Gebrehiwot Gebremichael, T. (2020). The potential role of astrocytes in Parkinson's disease (Pd). Med. Sci. (Basel) *8*, 7.

Ibanez, I., Diez-Guerra, F.J., Gimenez, C., and Zafra, F. (2016). Activity dependent internalization of the glutamate transporter glt-1 mediated by beta-arrestin 1 and ubiquitination. Neuropharmacology *107*, 376–386.

Juliano, R.L., Reddig, P., Alahari, S., Edin, M., Howe, A., and Aplin, A. (2004). Integrin regulation of cell signalling and motility. Biochem. Soc. Trans. *32*, 443–446.

Keller, B., La Harpe, R., and Garcia-Sevilla, J.A. (2017). Upregulation of iras/nischarin (I1-imidazoline receptor), A regulatory protein of mu-opioid receptor trafficking, in postmortem prefrontal cortex of long-term opiate and mixed opiate/cocaine abusers. Neurochem. Int. *108*, 282–286.

Kuijl, C., Pilli, M., Alahari, S.K., Janssen, H., Khoo, P.S., Ervin, K.E., Calero, M., Jonnalagadda, S., Scheller, R.H., Neefjes, J., and Junutula, J.R. (2013). Rac and Rab gtpases dual effector nischarin regulates vesicle maturation to facilitate survival of intracellular bacteria. Embo J. *32*, 713–727.

Lehre, K.P., and Danbolt, N.C. (1998). The number of glutamate transporter subtype molecules at glutamatergic synapses: chemical and stereological quantification in young adult rat brain. J. Neurosci. *18*, 8751–8757.

Levy, L.M., Attwell, D., Hoover, F., Ash, J.F., Bjoras, M., and Danbolt, N.C. (1998a). Inducible expression of the glt-1 glutamate transporter in A cho cell line selected for low endogenous glutamate uptake. Febs Lett. *422*, 339–342.

Levy, L.M., Warr, O., and Attwell, D. (1998b). Stoichiometry of the glial glutamate transporter glt-1 expressed inducibly in A Chinese hamster ovary cell line selected for low endogenous Na+-Dependent glutamate uptake. J. Neurosci. *18*, 9620–9628.

Li, F., Ma, H., Wu, N., and Li, J. (2016). Iras modulates opioid tolerance and dependence by regulating mu opioid receptor trafficking. Mol. Neurobiol. *53*, 4918–4930.

Li, S., Wu, N., Zhao, T.Y., Lu, G.Y., Wang, Z.Y., Li, F., and Li, J. (2019). The role of iras/nischarin involved in the development of morphine tolerance and physical dependence. Biochem. Biophys. Res. Commun. *512*, 460–466.

Lim, K.P., and Hong, W. (2004). Human nischarin/imidazoline receptor antisera-selected protein is targeted to the endosomes by A combined action of A px domain and A coiled-coil region. J. Biol. Chem. *279*, 54770–54782.

Marie, H., Billups, D., Bedford, F.K., Dumoulin, A., Goyal, R.K., Longmore, G.D., Moss, S.J., and Attwell, D. (2002). The amino terminus of the glial glutamate transporter glt-1 interacts with the Lim protein Ajuba. Mol. Cell Neurosci. *19*, 152–164.

Martinez-Villarreal, J., Garcia Tardon, N., Ibanez, I., Gimenez, C., and Zafra, F. (2012). Cell surface turnover of the glutamate transporter glt-1 is mediated by ubiquitination/deubiquitination. Glia *60*, 1356–1365.

Meeks, J.P., and Mennerick, S. (2007). Astrocyte membrane responses and potassium accumulation during neuronal activity. Hippocampus *17*, 1100–1108. https://doi.org/10.1002/hipo.20344.

Murphy-Royal, C., Dupuis, J., Groc, L., and Oliet, S.H.R. (2017). Astroglial glutamate transporters in the brain: regulating neurotransmitter homeostasis and synaptic transmission. J. Neurosci. Res. *95*, 2140–2151.

Murphy-Royal, C., Dupuis, J.P., Varela, J.A., Panatier, A., Pinson, B., Baufreton, J., Groc, L., and Oliet, S.H. (2015). Surface diffusion of astrocytic glutamate transporters shapes synaptic transmission. Nat. Neurosci. *18*, 219–226.

Peacey, E., Miller, C.C., Dunlop, J., and Rattray, M. (2009). The four major N- and C-terminal splice variants of the excitatory amino acid transporter glt-1 form cell surface homomeric and heteromeric assemblies. Mol. Pharmacol. *75*, 1062–1073.

Peterson, A.R., and Binder, D.K. (2019). Post-translational regulation of glt-1 in neurological diseases and its potential as an effective therapeutic target. Front Mol. Neurosci. *12*, 164.

Rose, E.M., Koo, J.C., Antflick, J.E., Ahmed, S.M., Angers, S., and Hampson, D.R. (2009). Glutamate transporter coupling to Na,K-atpase. J. Neurosci. *29*, 8143–8155.

Sekine-Aizawa, Y., and Huganir, R.L. (2004). Imaging of receptor trafficking by using alpha-bungarotoxin-binding-site-tagged receptors. Proc. Natl. Acad. Sci. U S A. *101*, 17114–17119.

Shimamoto, K., Sakai, R., Takaoka, K., Yumoto, N., Nakajima, T., Amara, S.G., and Shigeri, Y. (2004). Characterization of novel L-threo-beta-benzyloxyaspartate derivatives, potent blockers of the glutamate transporters. Mol. Pharmacol. *65*, 1008–1015. https://doi.org/10.1124/mol.65.4.1008.

Skarnes, W.C., Rosen, B., West, A.P., Koutsourakis, M., Bushell, W., Iyer, V., Mujica, A.O., Thomas, M., Harrow, J., Cox, T., et al. (2011). A conditional knockout resource for the genome-wide study of mouse gene function. Nature *474*, 337–342.

Smith, K.R., McAinsh, K., Chen, G., Arancibia-Carcamo, I.L., Haucke, V., Yan, Z., Moss, S.J., and Kittler, J.T. (2008). Regulation of inhibitory synaptic transmission by a conserved atypical interaction of GABA(A) receptor beta- and gamma-subunits with the clathrin AP2 adaptor. Neuropharmacology *55*, 844–850. https://doi.org/10.1016/j.neuropharm.2008.06.072.

Smith, K.R., Oliver, P.L., Lumb, M.J., Arancibia-Carcamo, I.L., Revilla-Sanchez, R., Brandon, N.J., Moss, S.J., and Kittler, J.T. (2010). Identification and characterisation of a Maf1/Macoco protein complex that interacts with GABAA receptors in

neurons. Mol. Cell Neurosci. *44*, 330–341. https://doi.org/10.1016/j.mcn.2010.04.004.

Sogaard, R., Borre, L., Braunstein, T.H., Madsen, K.L., and Macaulay, N. (2013). Functional modulation of the glutamate transporter variant Glt1b by the pdz domain protein Pick1. J. Biol. Chem. *288*, 20195–20207.

Tanaka, K., Watase, K., Manabe, T., Yamada, K., Watanabe, M., Takahashi, K., Iwama, H., Nishikawa, T., Ichihara, N., Kikuchi, T., et al. (1997). Epilepsy and exacerbation of brain injury in mice lacking the glutamate transporter glt-1. Science *276*, 1699–1702.

Tong, G., and Jahr, C.E. (1994). Block of glutamate transporters potentiates postsynaptic excitation. Neuron *13*, 1195–1203.

Twelvetrees, A.E., Yuen, E.Y., Arancibia-Carcamo, I.L., MacAskill, A.F., Rostaing, P., Lumb, M.J., Humbert, S., Triller, A., Saudou, F., Yan, Z., and Kittler, J.T. (2010). Delivery of GABAARs to synapses is mediated by HAP1-KIF5 and disrupted by mutant huntingtin. Neuron *65*, 53–65. https://doi.org/10.1016/j.neuron.2009.12.007.

Underhill, S.M., Wheeler, D.S., and Amara, S.G. (2015). Differential regulation of two isoforms of the glial glutamate transporter eaat2 By Dlg1 and camkii. J. Neurosci. *35*, 5260–5270.

Volterra, A., Bezzi, P., Rizzini, B.L., Trotti, D., Ullensvang, K., Danbolt, N.C., and Racagni, G. (1996). The competitive transport inhibitor L-trans-pyrrolidine-2, 4-dicarboxylate triggers excitotoxicity in rat cortical neuron-astrocyte co-cultures via glutamate release rather than uptake inhibition. Eur. J. Neurosci. *8*, 2019–2028. https://doi.org/10.1111/j.1460-9568.1996.tb01345.x.

Wadiche, J.I., Amara, S.G., and Kavanaugh, M.P. (1995a). Ion fluxes associated with excitatory amino acid transport. Neuron *15*, 721–728.

Wadiche, J.I., Arriza, J.L., Amara, S.G., and Kavanaugh, M.P. (1995b). Kinetics of A human glutamate transporter. Neuron *14*, 1019–1027.

Zerangue, N., and Kavanaugh, M.P. (1996). Flux coupling in A neuronal glutamate transporter. Nature *383*, 634–637.

Zou, S., Pita-Almenar, J.D., and Eskin, A. (2011). Regulation of glutamate transporter Glt-1 By magi-1. J. Neurochem. *117*, 833–840.

STAR★METHODS

KEY RESOURCES TABLE

REAGENT or RESOURCE	SOURCE	IDENTIFIER
Antibodies		
Rabbit IgG control	ThermoFisher Scientific	Cat# 10500C; RRID: AB_2532981
Mouse IgG control	ThermoFisher Scientific	Cat# 10400C; RRID: AB_2532980
Mouse-anti-EEA1	BD Transduction Labs	Cat# 610457; Clone# 14/EEA1; RRID: AB_397830
Mouse-anti-Nischarin,	BD Transduction Labs	Cat# 558262 RRID: AB_397069
Mouse-anti-V5	Thermofisher Scientific (Invitrogen)	Cat# R960-25 RRID: AB_2556564
Rabbi-anti-EAAT2 (GLT-1)	Alomone Labs	Cat# AGC-022 RRID: AB_2039891
Rabbit-anti-GFP	SantaCruz	Cat# sc-8334; RRID: AB_641123
Rat-anti-GFP	Nacalai Tesque	Cat# 04404-84; RRID: AB_10013361
Mouse-anti-GST (supernatant)	Neuromab	Cat# 75-148; clone# N100/13; RRID: AB_10671817
Mouse-anti-HA-tag	Produced and purified in house from hybridoma cells. Vendor: James Trimmer, UC Davis	Clone# 12CA5; RRID: AB_253207
Goat-anti-rabbit IgG (H+L), HRP	Jackson ImmunoResearch	Cat# 111-035-003; RRID: AB_2313567
Goat-anti-mouse IgG (H+L), HRP	Jackson ImmunoResearch	Cat# 115-035-003; RRID: AB_10015289
Goat anti-mouse IgG (light chain specific), HRP	Jackson ImmunoResearch	Cat# 115-035-174; RRID: AB_2338512
Donkey-anti-mouse AlexaFluor 488	Jackson ImmunoResearch	Cat# 715-545-151; RRID: AB_2341099
Donkey-anti-rabbit AlexaFluor 488	ThermoFisher Scientific	Cat# A-21206; RRID: AB_2535792
Goat-anti-mouse Alexa Fluor 488	ThermoFisher Scientific	A32723 RRID: AB_2633275
Donkey-anti-rat AlexaFluor 488	ThermoFisher Scientific	Cat# A-21208; RRID: AB_141709
Donkey-anti-mouse Alexa Fluor 594	ThermoFisher Scientific	A32744 RRID: AB_2762826
Goat-anti-mouse AlexaFluor 555	ThermoFisher Scientific	Cat# A-21424; RRID: AB_141780
Goat-anti-rabbit AlexaFluor 555	ThermoFisher Scientific	Cat# A-21430; RRID: AB_2535851
Donkey-anti-mouse AlexaFluor 647	ThermoFisher Scientific	Cat# A-31571; RRID: AB_162542
Donkey-anti-rabbit AlexaFluor 647	ThermoFisher Scientific	Cat# A-31573; RRID: AB_2536183
Bacterial and virus strains		
One Shot TOP10 Chemically Competent *E.coli*	Invitrogen	Cat# C404010
BL21(DE3) One Shot Chemically Competent *E.Coli*	Invitrogen	Cat# C600003
Critical commercial assays		
BioRad protein assay	BioRad	Cat# PI-23225
Gateway™ LR Clonase™ Enzyme Mix	ThermoFisher Scientific	Cat# 11791019
In-Fusion® HD Cloning Plus	Takara	Cat# 638909
Duolink™ PLA Technology	Sigma Aldrich	Cat# DUO92101
Chemicals, peptides, and recombinant proteins		
Hank's Buffered Salt Solution (HBSS)	GIBCO	Cat# 14180046
1M HEPES buffer	GIBCO	Cat# 15630080
Minimal Essential Medium (MEM)	GIBCO	Cat# 31095029

(*Continued on next page*)

Continued

REAGENT or RESOURCE	SOURCE	IDENTIFIER
Heat inactivated Horse Serum (HRS)	GIBCO	Cat# 26050088
Sodium pyruvate	GIBCO	Cat# 11360070
Glucose	GIBCO	Cat# A2494001
Neurobasal medium	GIBCO	Cat# 21103049
B-27	GIBCO	Cat# 17504044
GlutaMAX	GIBCO	Cat# 35050061
DMEM (high glucose)	GIBCO	Cat# 41965039
Fetal Bovine Serum	GIBCO	Cat# 10082147
Penicillin/Streptomycin	GIBCO	Cat# 15140122
2.5% Trypsin	GIBCO	Cat# 15090046
DNase	Sigma-Aldrich	Cat# DN-25
Poly-L-lysine (PLL)	Sigma-Aldrich	Cat# P6282-5MG
Lipofectamine-2000	Invitrogen	Cat# 11668027
IPTG	Melford	Cat# 367-93-1
PMSF	AppliChem	Cat# A0999,0025
Antipain	Peptide	Cat# 4062
Pepstatin	Peptide	Cat# 4397
Leupeptin	Peptide	Cat# 4041
Glutathione Sepharose 4B	GE Healthcare	Cat# 17075601
Propidium Iodide	Thermofisher Scientific	Cat# P1304MP
Protein A Sepharose	Generon	Cat# PC-A25
GFP-Trap	Chromotek	Cat# gta-100
Luminate Crescendo Western HRP substrate	Milipore	Cat# WBLUR0500
ProLong Gold antifade reagent	Invitrogen	Cat# P36930
NaCl	Fisher Scientific	S/3161/60
HEPES	Sigma-Aldrich	H3375
D-(+)-glucose	Fisher Scientific	G/0S00/53
KCL	Sigma-Aldrich	PS405
$CaCl_2$	Sigma-Aldrich	C7902
NaH_2PO_4	British Drug Houses	1024S4R
$MgCl_2$	VWR Chemicals	25108.260
(+)-Bicuculline	Sigma-Aldrich	14340
D-AP5	Sigma-Aldrich	A8054
(+)MK-801	Tocris	0924
NBQX disodium salt	Tocris	1044/1
Barium chloride	Sigma-Aldrich	B0750
D-aspartic acid	Tocris	0213
TFB-TBOA	Tocris	2532/1
Potassium D-gluconate	Sigma-Aldrich	G4500
EGTA	Sigma-Aldrich	E4378
MgATP	Sigma-Aldrich	A9187
Na_2GTP	Sigma-Aldrich	G8877
KOH	British Drug Houses	10210
Experimental models: Cell lines		
COS-7	ATCC	Cat# CRL-1651; RRID: CVCL_0224
HeLa	ATCC	Cat# CRM-CCL-2; RRID: CVCL_0030

(*Continued on next page*)

Continued

REAGENT or RESOURCE	SOURCE	IDENTIFIER
Experimental models: Organisms/strains		
Wild-type Sprague-Dawley rats	Charles River	N/A
GLT-1 knockout	Tanaka et al., 1997	N/A
Nischarin transgenic (HEPD0811_2_A03; Allele: Nischtm1a(EUCOMM)Hmgu)	Wellcome Trust Sanger Institute as part of the International Knockout Mouse Consortium (IKMC) (Skarnes et al., 2011)	N/A
Oligonucleotides		
Subcloning to create GLT1aBBS forward primer: ccctggagccctaccctgacCCATCTGAGGAGGCC	This paper	N/A
Subcloning to create GLT1aBBS reverse primer: agctctcgtagtatctccaaGGTGCCACCAGAACTTT	This paper	N/A
Subcloning to generate GFP-Nisch forward primer: ATCATTTTGGCAAAGCTAGCaccatggcggctgcgacact	This paper	N/A
Subcloning to generate GFP-Nisch reverse primer: CGTCGACTGCAGAATTCtgccagtgagctccacaggc	This paper	N/A
Deletion to generate GFP-Δphox forward primer: GTAAATGGTGTCACTGCAGCACT	This paper	N/A
Deletion to generate GFP-Δphox reverse primer: CTCAGGGCCGAAGCTGAGTGT	This paper	N/A
Deletion to generate GFP-phox forward primer: GGCCTCATGGGCCCAG	This paper	N/A
Deletion to generate GFP-phox reverse primer: TTCATAGAGGTGAAAATGCAGGA	This paper	N/A
Recombinant DNA		
pcDNA3.1-GLT1aV5	Peacey et al., 2009	N/A
pcDNA3.1-GLT1aHA	Peacey et al., 2009	N/A
pcDNA3.1-GLT1aBBS	This paper	N/A
Mouse Nischarin vector	I.M.A.G.E. Consortium	clone ID: 100068156
CAG-GFP	Addgene	Cat# 16664
GFP-Nisch	This paper	N/A
GFP-Δphox	This paper	N/A
GFP-phox	This paper	N/A
Software and algorithms		
Fiji/ImageJ	National Institutes of Health	https://imagej.net/Welcome RRID: SCR_003070
Metamorph	Molecular Devices	N/A
ZEN LSM	Zeiss	N/A
GraphPad Prism	GraphPad Software	N/A
Axon pCLAMP 10	Axon Instruments	NA

RESOURCE AVAILABILITY

Lead contact

Further information and requests for resources and reagents should be directed to and will be fulfilled by the Lead Contact Dr Josef Kittler (j.kittler@ucl.ac.uk).

Materials availability

Plasmids generated as part of this study will be made available upon request.

Data and code availability

All data reported in this paper will be shared by the lead author upon request.

This paper does not report original code.

Any additional information required to reanalyze the data reported in this paper is available from the lead contact upon request.

EXPERIMENTAL MODEL AND SUBJECT DETAILS

Cell culture

Primary cultures of rat cortical astrocytes were prepared from E18 or P0 Sprague-Dawley rats as previously described (Banker, 1998). Hippocampal astrocyte-neuron rat co-cultures were obtained from E18 rat embryos as described previously with some modifications (Arancibia-Carcamo et al., 2009). The sex of each rat was not verified. Embryonic astrocyte-neuron hippocampal co-cultures were prepared from nischarin WT or KO mice embryos at 16 days post-fertilization. The sex of each mouse embryo was not verified. All experimental procedures were carried out in accordance with UCL institutional animal welfare guidelines and licensed by the UK Home Office in accordance with the Animals (Scientific Procedures) Act 1986. COS7 and HeLa cells were maintained in 10cm dishes containing 10 mL Enhanced Dulbecco's Modified Eagles Medium (DMEM), supplemented with pen/strep and 10% FBS, at 37°C and 5% CO2,

Transgenic animal

The *Nisch* (HEPD0811_2_A03; Allele: *Nisch*$^{tm1a(EUCOMM)Hmgu}$) mouse line was obtained from the Wellcome Trust Sanger Institute as part of the International Knockout Mouse Consortium (IKMC) (Skarnes et al., 2011). The *Nisch* transgenic line was generated following the Knockout-First strategy on C57BL/6N Taconic strain. A L1L2_Bact_P cassette encoding an engrailed1 splice acceptor sequence, a LacZ reporter and a Neomycin resistance gene was inserted between exons 4 and 5 disrupting *Nisch* transcription. Animals were maintained under controlled conditions (temperature 20 ± 2°C; 12 h light-dark cycle). Food and water were provided *ad libitum*. The genotyping was carried out following Sanger's recommended procedures, briefly the DNA was extracted from ear biopsies and PCRs were performed with the following primers (5' to 3'): Nisch_5arm_WTF: AGAGGCCCAGAGACCTGATA; Nisch_Crit_WTR: TGGACACGTGATGAGAAAGG; 5mut_R1: GAACTTCGGAATAGGAACTTCG; LacZ_2_small_F: ATCACGACGCGCTGTATC; LacZ_2_small_R: ACATCGGGCAAATAATATCG. All experimental procedures were carried out in accordance with UCL institutional animal welfare guidelines and licensed by the UK Home Office in accordance with the Animals (Scientific Procedures) Act 1986.

METHOD DETAILS

Yeast two-hybrid screen

This screen was done as described previously (Marie et al., 2002). Briefly, bait cDNA for the GLT-1 N terminus (amino acids 1–44 of the rat protein sequence) was cloned into the yeast expression vector pPC97 in frame with the GAL4 binding domain. It was screened against a random-primed cDNA library from seizure-stimulated adult rat hippocampus cloned in the yeast expression vector pPC86 in frame with the GAL4 activation domain. Interacting proteins were identified by colony selection on plates lacking leucine, tryptophan, and histidine and confirmed by using a β-galactosidase assay and by checking that in the absence of GLT-1 bait the library protein did not activate the reporter genes (*His3,* allowing growth on histidine-deficient medium, and *LacZ,* expressing β-galactosidase).

Plasmid constructs

Mouse GLT-1a cDNA with V5 and HA epitope tag inserted into the extracellular loop of the transporter (between Pro^{199} and Pro^{200}) and cloned into pcDNA3.1- was gifted by Dr. M. Rattray (Peacey et al., 2009). Bungarotoxin binding sequence (BBS) tag was introduced by PCR into GLT-1a and 1b between the two proline residues (P199 and P200) in the extracellular loop using the following primers (written 5' to 3'): *ccctggagccctaccctgacCCATCTGAGGAGGCC*; *agctctcgtagtatctccaaGGTGCCACCAGAACTTT*, where lowercase text corresponds to the sequence of the BBS tag. Mouse Nischarin vector (clone ID: 100068156) was obtained from I.M.A.G.E. Consortium. The phox domain of Nischarin was deleted using the following primers: GTAAATGGTGTCACTGCAGCACT, CTCAGGGCCGAAGCTGAGTGT. The

dominant negative, phox vector was generated using the following primers: GGCCTCATGGGCCCAG, TTCATAGAGGTGAAAATGCAGGA. The full length Nischarin, Dphox and phox vectors were C-terminally tagged with GFP by infusion cloning in frame into CAG-GFP (Addgene) using the following primers: ATCATTTTGGCAAAGCTAGCaccatggcggctgcgacact and CGTCGACTGCAGAATTCtgccagtgagctccaca ggc, where lowercase text corresponds to parts of the Nischarin sequence.

Preparation and transfection of astrocyte cultures

Primary cultures of cortical astrocytes were prepared from E18 or P0 Sprague-Dawley rats as previously described (Banker, 1998). Cells were maintained in Dulbecco's modified Eagle's medium DMEM GlutaMAX (Invitrogen) supplemented with 4.5 g/L glucose, 20% fetal bovine serum, 10 u/ml penicillinG, and 100 μg/ml streptomycin at 37°C with 5% CO2 in a humidified incubator. Media was exchanged the day after plating. Astrocytes were passaged when confluency was reached (10 days after plating). For biotinylation assay, astrocytes were transfected with GLT-1aV5 and GFP (2μg, 1μg) or GLT-1aV5 and GFP-Nisch (2μg, 2μg) using Amaxa Nucleofector® technology following the manufacturer's protocol and maintained for 5 to 7 days before processing.

Preparation and transfection of mixed culture and the neuron-astrocyte co-cultures

Hippocampal cultures were obtained from E18 rat embryos as described previously with some modifications (Arancibia-Carcamo et al., 2009). In order to enrich the culture with astrocytes, the neurons were kept 24h after plating in attachment medium (Minimal Essential Medium, 10% Horse Serum, 1 mM Sodium Pyruvate and 0.6% Glucose) before replacing with maintenance medium (Neurobasal Medium, B27 supplement, Glutamax, 0.6% Glucose, Penstrep). For live and fixed time lapse confocal and SIM imaging, astrocytes were transfected by nucleofection with GLT-1aBBS and GFP-Nisch (2μg, 2μg) or GLT-1aBBS and GFP (2μg, 1μg) (Amaxa Nucleofector) and plated on top of DIV10 hippocampal neurons. Transfected astrocytes were maintained with neurons for 3 to 4 days before imaging.

Cell culture and transfection

COS7 and HeLa cells were maintained in 10cm dishes containing 10 ml Enhanced Dulbecco's Modified Eagles Medium (DMEM), supplemented with pen/strep and 10% FBS, at 37°C and 5% CO2, transfected by nucleofection using an Amaxa electroporator and allowed 24-48 h for protein expression.

Coimmunoprecipitation assays from rat brain homogenate and cell culture

Coimmunoprecipitation experiments from brain/cell culture were performed as previously described (Twelvetrees et al., 2010). Briefly, mouse brain/cell culture expressing proteins of interest was homogenised in pull- down buffer (50 mM TRIS pH 7.5, 0.5 % triton X-100, 150 mM NaCl, 1 mM EDTA, 1mM PMSF with antipain, pepstatin and leupeptin at 10 μg/ml) and solubilised for 2 hours. Solubilised material was ultracentrifuged at 66,000 g for 40 min at 4°C and the supernatant (solubilised protein) was incubated with 2μg of anti-GLT1 (Alomone, Cat No: AGC022) antibody overnight at 4°C. To precipitate complexes, 20 μl protein-A or –G beads or GFP trap beads (Chrometek) were added for 1 hour at 4°C. Beads were then washed extensively and bound complexes were analysed by SDS-PAGE and western blotting.

Western blotting

SDS - polyacrylamide gel electrophoresis (PAGE) and Western Blotting samples were denatured at 94°C for 5 minutes in 3 x SDS sample buffer (150mM Tris pH 8, 6% SDS, 0.3M DTT, 0.3% Bromophenol Blue, 30% glycerol). Polyacrylamide gels were prepared using 10% running gels and 5% stacking gels in Novex 1.5mm Cassettes and run using the Novex XCell SureLock Mini-Cell system. Gels were transferred onto Hybond-C nitrocellulose membrane (GE Healthcare). Membranes were blocked in 4% milk for 1 h and incubated overnight at 4°C with shaking in the appropriate primary antibody against Nischarin (1:500, BD Biosciences, Cat No: 558262), GFP (1:500, Santacruz, Cat No: sc-8334), V5 (1:2000, Invitrogen, Cat. No: R960-25), GLT (1:500, Alomone). HRP-conjugated secondary antibodies were from Rockland (1:10,000). Bands were visualised using Crescendo Chemiluminescent substrate (Millipore) together with an ImageQuant LAS 4000 CCD camera system (GE Healthcare).

GST pull down assays from transfected COS7 cells

GST fusion with amino acids 1–44 of the N terminus of GLT-1 (GST–GLT-N), C terminus of GLT-1 (GST-GLT-C) and C terminus of GLAST (GST-GLAST-C), GST fusions A–E, encoding amino acids 1–15, 15–30,

30–44, 9–23, and 23–37 of GLT-1 were cloned as described previously (Marie et al., 2002). Pull-downs from brain were performed as described previously (Smith et al., 2008, 2010). Briefly, COS cells transfected with GFP-Nisch (2μg) was homogenized in pull-down buffer (50 mM HEPES, pH 7.5, 0.5% Triton X-100, 150 mM NaCl, 1 mM EDTA, and 1 mM PMSF with antipain, pepstatin, and leupeptin at 10g/ml) and solubilized for 2 h. Solubilized material was ultracentrifuged at 66,000g for 40 min at 4°C, and the supernatant (solubilized protein) was exposed to 10–20μg of GST fusion protein attached to glutathione–agarose beads for 1 h at 4°C. Beads were then washed extensively and analyzed by SDS-PAGE and western blotting.

Biotinylation assay

Surface biotinylation assays have been fully described previously (Smith et al., 2010; Twelvetrees et al., 2010). Briefly confluent astrocyte cultures were incubated on ice with biotin solution (Sulpho-NHS-biotin(PIERCE) at 0.5 mg/ml in PBS containing Ca^{2+} /Mg^{2+}) and quenched with quench buffer (PBS Ca2+/Mg2+containing 1 mg/ml BSA). Astrocytes were solubilised for 1 h in RIPA buffer (50 mM Tris pH 7.5, 1mM EDTA, 2 mM EGTA, 150 mM NaCl, 1% NP40, 0.5% DOC, 0.1% SDS, and 1 mM PMSF with anti-pain, pepstatin and leupeptin 10μg/ml) and the lysates were then centrifuged to pellet cell debris. 15% of the supernatant was taken to use as a total protein sample and the remainder was incubated for 2h with 25μl Ultralink immobilized NeutrAvidin (PIERCE) 50% slurry at 4°C to precipitate biotin labeled membrane proteins. Beads were washed three times in RIPA buffer and analysed by SDS-PAGE and western blotting. Biotinylated surface GLT-1 transporters were identified by using anti-GLT primary antibody (1:500, Alomone) or anti-V5 primary antibody (1:2000, Invitrogen) and detection of enhanced chemilluminescence from HRP-coupled anti-rabbit secondary antibodies followed by detection with an ImageQuant LAS4000 mini imaging system and analysis with ImageQuant software (GE Healthcare).

Excitotoxicity assay

DIV14 hippocampal cultures were treated for 20 min with 10μM Glutamate and 10μM Glycine before replacement with conditioned maintenance media. 24 h later, cultures were treated with 10μg/mL Propidium Iodide (PI) for 10 min prior to fixation for 5 min with 4% PFA at room temperature. Cell nuclei were stained with DAPI. Coverslips were imaged by confocal microscopy using a 10x objective (0.8x digital zoom, 4 averaging, 1024 × 1024, bit depth 8). Laser power and gain were kept consistent within and across all experiments. Images were analysed using ImageJ Cell Counter plugin, manually counting DAPI + ve cells and PI + ve cells in the same field of view. 3-4 field of views were taken per coverslip, 3-6 coverslips taken per embryo. N= 3 litter-matched embryos from separate preps. Experiments were performed blinded during image acquisition and analysis.

Proximity ligation assay

The *in-situ* proximity ligation assay (PLA) was used according to the manufacturer's instructions (Olink Bioscience). Neurons were fixed in 4% PFA/30% sucrose, blocked (10% horse serum, 0.5% BSA, and 0.2% Triton X-100, 10 min at room temperature), and incubated with primary antibodies (1:500, anti-GLT (gift from Dr. N.Danbolt) and anti-Nischarin (1:100, Sigma, Cat. No: HPA023189). For control PLA, single primary antibody was applied. Cells were washed in 1 × PBS and then incubated with secondary antibodies conjugated to oligonucleotides. Ligation and amplification reactions were conducted at 37°C, before mounting and visualization with confocal laser scanning microscope. Images were thresholded and number of puncta and DAPI stained nuclei were manually counted for each image using the *Metamorph software*. Experiments were performed blinded during image acquisition and analysis.

Antibody feeding

For receptor internalization and recycling assays, HeLa cells were transfected with GFPNisch and GLT-1a-HA (2μg, 2μg) or GFP and GLT-1a-HA (1μg, 2μg). The transporters were live labeled with anti-HA antibody in DMEM +25mM HEPES at 17°C. Labelled transporters were allowed to internalize for 60 min at 37°C. For recycling assay, surface transporters were stripped using acid wash (0.2M acetic acid and 0.5M NaCl). Cells were then returned to the incubator for 30 and 60 min at 37°C to allow internalized transporters to recycle to the surface. For surface staining, cells were fixed with 4% paraformaldehyde (PFA)/4% sucrose/PBS, pH 7, for 5 min and blocked with block solution (PBS, 10% horse serum, and 0.5% BSA) for 10 min, followed by Alexa Fluor-555-conjugated anti-mouse secondary antibody for 1h (1:400; Invitrogen). For identifying internalized transporters, cells were subsequently permeabilized with block solution containing 0.2% Triton X-100 for 10min, followed by Alexa Fluor-555-conjugated anti-mouse secondary antibody

(1:1000; Invitrogen). After extensive washing, coverslips were mounted on microscope slides using ProLong Gold antifade reagent (Invitrogen) and sealed with nail varnish. Images were attained using the confocal laser scanning microscope. Image analysis was performed using *ImageJ* software. For quantification of receptor internalization, red fluorescence that was not colocalized with cyan fluorescence (surface receptors) was calculated as the internalized transporter population or vice versa for calculating the surface transporter population in the recycling assay and normalized to total transporter population. Rate of internalization/recycling at different time points is measured as fold change relative to 0min.

Immunostaining

Hippocampal cell culture was fixed with 4% PFA/4% sucrose/PBS, pH7, for 5min. The cells were permeabilized with block solution (PBS, 10% horse serum, and 0.5% BSA, 0.2% Triton) for 10min. The cells were incubated with primary antibodies including, anti-GLT1 (1:500, Alomone), anti-EEA1 (1:500, BD Bioscience, Cat. No: 610456), anti-Map2 (1:1000) for 1hr in block solution, followed by incubation with Alexa Fluor 488 or 555 or 647- conjugated secondary antibodies (1:1000, Invitrogen) for 1h. After extensive washing, coverslips were mounted on microscope slides using Pro-Long Gold antifade reagent (Invitrogen) and sealed with nail varnish. Images were attained using Zeiss LSM 700 upright confocal microscope with an Apochromat 63× oil immersion lens with 1.4 numerical aperture. Images were digitally captured using ZEN software with excitation at 488nm for GFP and Alexa Fluor 488, 555nm for Alexa Fluor 555 and 633nm for Alexa Fluor 647 and conjugated secondary antibodies. Pinholes were set to 1 Airy unit creating an optical slice of 0.8μm. For measuring colocalization, the colocalization plugin of the *Metamorph* software was used. Fluorescence intensity was measured using the *ImageJ* software.

Live imaging

Structured Illumination Microscopy was performed using a Zeiss Elyra PS.1 equipped with 488, 555 and 642 nm lasers. Images were acquired with 63 × 1.4 NA oil immersion objective using pco.edge sCMOS camera and Zen 2012 image analysis software. Typically, images were acquired with 51μm grating and 3 rotations by exciting fluorophores with 1–3% laser intensity and 120-150 ms exposure time. Post-acquisition, images were processed with Zen 2012 using the SIM reconstruction module with default settings and drift corrections between the channels were performed with respect to 100nm Tetraspec fluorescent microspheres (Molecular probes). To create kymographs image sequences were opened within ImageJ. Curved processes were straightened using the "straighten" macro and kymographs created by the "multiple kymograph" macro. Resultant kymographs show the process along the x axis and time across the y axis.

Electrophysiology

Electrophysiology was carried out on embryonic hippocampal cultures on their tenth day *in vitro*. Cultures were prepared from nischarin WT or KO mice embryos at 16 days post-fertilization. Recordings were carried out at room temperature (20-21°C) with a HEPES-buffered extracellular solution mimicking cerebrospinal fluid (artificial cerebrospinal fluid, aCSF) containing (in mM): 140 NaCl, 10 HEPES, 10 glucose, 2.5 KCl, 2 $CaCl_2$, 1 NaH_2PO_4, 1 $MgCl_2$, pH 7.4 adjusted to with NaOH, osmolarity 300 mOsm (oxygenated with 100% O_2). The solution was perfused at a flow rate of 3-4 ml/min through the recording chamber using gravity-driven perfusion from syringe barrels (60ml) connected to individual tubes, which merged into a single outlet just prior to reaching the bath. Whole-cell patch-clamp recordings were made from astrocytes using a potassium gluconate based internal solution, containing (in mM): 130 K-gluconate, 4 NaCl, 10 HEPES, 1 $CaCl_2$, 10 EGTA, 2 MgATP, 0.5 Na_2GTP (adjusted to pH 7.1–7.2 with KOH, and osmolarity ~ 285 mOsm). Alexa Fluor 594 (20 μM) was added to each aliquot of internal solution on the day of the experiment. Astrocytes were recognised visually by their low contrast soma, with an angular morphology and stellate processes revealed by dye-filling and usually gap junctional coupling allowing dye spread to other nearby astrocytes (Figure 4C).

Recording glutamate uptake in astrocytes

In order to record the glutamate uptake current from astrocytes, voltage-clamp recordings were made at the cell's resting potential (typically around −90 mV). D-aspartate (200 μM, Sigma) was used to evoke a transporter current, since it is taken up by glial glutamate transporters (Davies and Johnston, 1976; Barbour et al., 1991; Furness et al., 2008) and may have less effect than glutamate on glutamate receptors. However, D-aspartate may activate NMDA receptors or inhibit AMPA/KA receptors (Gong et al., 2005), or release

glutamate via heteroexchange on transporters (Volterra et al., 1996). Any resulting activation of glutamate receptors might cause membrane potential depolarisation, neuronal action potentials and a rise of $[K^+]_o$ into the extracellular space, which could evoke an inward current in astrocytes (which have a highly K^+-permeable membrane: Meeks and Mennerick, 2007). To prevent these effects we therefore supplemented the aCSF with a selection of blockers, which were present throughout the experiment: TTX to block action potentials (150nM, Tocris), a $GABA_A$ receptor blocker (bicuculline 10 μM, Sigma), NMDA receptor blockers (D-AP5 50 μM, Tocris; (+)MK-801 10 μM, Sigma; 5,7-DCK 10 μM, Sigma), an AMPA and kainate receptor blocker (NBQX 10 μM, Sigma), and an inwardly rectifying potassium channel blocker (barium chloride 200 μM, Sigma) which does not affect glutamate transport (Barbour et al., 1991). A non-transported glial glutamate transporter blocker (Shimamoto et al., 2004), TFB-TBOA (10 μM, Tocris) was also used in some experiments to block the glutamate transporter current evoked by D-aspartate. The size of the uptake current was calculated as the inward current recorded in D-aspartate minus the average of the baseline currents measured before and after D-aspartate application (using Clampfit 10.4). Experiments were performed with the experimenter blinded to the genotype.

QUANTIFICATION AND STATISTICAL ANALYSIS

All experiments were performed on astrocytes/cell culture/mixed hippocampal astrocyte-neuron co-culture from at least three individual preparations. For all quantified experiments the experimenters were blind to the condition of the sample analyzed. All image analysis was performed blinded. Values are given as mean ± standard error of the mean (SEM). Error bars represent SEM. Statistical analysis was performed in GraphPad Prism (version 8; GraphPad Software, CA, USA) or Microsoft Excel. All data was tested for normal distribution with D'Agostino & Pearson test to determine the use of parametric (Student's t test, one-way ANOVA) or non-parametric (Mann-Whitney, Kruskal-Wallis) tests. When $p < 0.05$, appropriate post hoc tests were carried out in analyses with multiple comparisons and are stated in the figure legends.